PERGAMON

International Journal of Impact Engineering 24 (2000) 117–131

INTERNATIONAL JOURNAL OF IMPACT ENGINEERING

www.elsevier.com/locate/ijimpeng

Carbon content effect on high-strain-rate tensile properties for carbon steels

Masaaki Itabashi*, Kozo Kawata

Department of Materials Science and Technology, Faculty of Industrial Science and Technology, Science University of Tokyo, 2641, Yamazaki, Noda, Chiba 278-8510, Japan

Received 6 May 1997; received in revised form 6 August 1999

Abstract

For the improvement or development of more crashworthy metallic materials, the effect of each chemical composition on stress–strain behavior under dynamic tension should be understood phenomenologically. Such knowledge is essential for alloy designers and engineers. Formerly, the present authors constructed a high-velocity tensile loading machine of a horizontal slingshot type to obtain dynamic tensile stress–strain relationships for structural materials, such as metallic alloys, plastics and composites at the strain rate of $1 \times 10^3\ s^{-1}$. This strain rate is of the same order of a car crash on the street. Using this apparatus and a usual material testing machine, seven structural carbon steels of C content ranging 0.14–0.54 wt% were tested at four strain rates of 1×10^{-3}, 1×10^{-2}, 1×10^{-1} and $1 \times 10^3\ s^{-1}$. From the stress–strain curves obtained, the effect of the strain rate and C content on mechanical properties for the steels were evaluated. Especially, even at the high strain rate, the yield stress and ultimate strength of the steels could be predicted by an empirical equation for quasi-static tensile tests in consideration of C and Mn contents.

Keywords: Carbon steel; High strain rate; Alloy design; One bar method; C content

1. Introduction

Crashworthiness of traffic vehicles is essential to save occupants' lives in an accident. The process of crashing energy absorption must be evaluated correctly and properly reflected in structural design. Mechanical characterization for structural materials in dynamic uniaxial tensile loading

* Corresponding author. Tel.: + 81-471-24-1501 ext.4321; fax: + 81-471-23-9362.
E-mail address: itabashi@rs.noda.sut.ac.jp (M. Itabashi)

0734-743X/00/$ - see front matter
PII: S0734-743X(99)00050-0

condition is one of the most practical themes to be investigated thoroughly. Manjoine and Nadai [1] carried out a systematic work on high-velocity tensile tests for copper at temperatures ranging from room temperature to 1000°C. This is one of the pioneering works in the development of dynamic tensile test method. Duwez and Clark [2] constructed a high-velocity tensile loading machine of a rotating wheel type and confirmed the accuracy of their load cell which was referred as a dynamometer with plastic wave propagation theory. Clark and Duwez [3] constructed another hydraulic tensile testing machine. The strain rate dependence of the proportional limit and ultimate strength of eight steels were reported at the strain rate range of 40–200 s^{-1}. On the other hand, dynamic compressive testing technique was also developed independently. Taylor developed the well-known Taylor impact test [4] and Whiffin executed the tests for many steels [5]. The experimental results showed that there was a linear relationship between the logarithmic quasi-static yield stress and the ratio of the dynamic yield stress to quasi-static one. This test method has been further revised to obtain more information from this simple technique [6]. Kolsky established the split Hopkinson pressure bar (SHPB) method to obtain dynamic compressive stress–strain curves [7]. The SHPB method was rearranged to realize the dynamic tensile loading by Harding et al. [8], Lindholm and Yeakly [9] and Nicholas [10]. Holzer summarized the history of the dynamic material testing up to 1978 [11].

From the viewpoint of constitutive equations of a wide strain rate range, Malvern proposed a constitutive equation of the well-known Malvern type for a hardened aluminum alloy, introducing the over stress [12]. Seeger proposed a constitutive equation of the thermal activation type [13]. Tanaka and Nojima carried out constant strain rate tests and incremental strain rate change tests and derived a constitutive equation of the Seeger type for a low carbon steel and a structural steel [14]. In order to represent the yield phenomenon, Johnston and Gilman [15] and Gillis and Gilman [16,17] constructed constitutive equations of the Johnston–Gilman type, introducing micromechanical variables for LiF crystal. This type of the constitutive equation was applied to steel by Hahn [18]. Kuriyama and Kawata refined the equation for mild steel, introducing plastic flow functions [19]. The above-mentioned constitutive equations are further refined by many investigators. However, in order to introduce the dynamic tensile/compressive stress–strain relationships to computer codes, there are two ways. In most cases an empirical equation like the Cowper–Symonds equation is introduced [20] and in a few cases a suitable constitutive equation based on the preliminary experiments of the interested materials is introduced. This paper contributes to the former case.

So far, many metallic materials have been investigated under high-velocity tension, compression, torsion and shear. The investigated materials seemed to tend to pure metals and specially focused alloys from the viewpoint of physics and metallurgy. On the other hand, the demand from mechanical engineers and structural designers have been focused on the dynamic behavior of more practical alloys, for example, carbon steels, stainless steels, strengthened aluminum alloys, etc. For the improvement or development of more crashworthy materials and structures, the effect of each chemical composition on not only Charpy or Izod impact values but also dynamic stress–strain behavior should be recognized. The present authors formerly investigated that C content (0.033–0.21 wt%) effect on dynamic tensile behavior at the strain rate of 1×10^3 s^{-1} for carbon steels and Ni content (8.97–13.54 wt%) effect on austenitic stainless steels [21]. For the latter case, Ni content had the opposite effects between quasi-static and dynamic strain rates on strength, elongation and absorbed energy. Such knowledge is essential for alloy designers.

In this paper, with the dynamic tensile testing machine of a slingshot type and the usual material testing machine, seven structural carbon steels of higher C content range (0.14–0.54 wt%) were tested at four strain rates ($\dot{\varepsilon} = 1 \times 10^{-3}$, 1×10^{-2}, 1×10^{-1} and 1×10^{3} s^{-1}). From the stress–strain curves, the effects of strain rate and C content on strength, elongation and absorbed energy were evaluated. For the variation of the strength with increasing strain rate, not only the C content but also the Mn content should be introduced to predict the strength of the steels consisting of ferritic and pearlitic phases.

2. Experimental

The demand from the fields of plastic working and forging are recently focused on the constitutive relation at $\dot{\varepsilon} = 10^{0}$–$10^{2}$ s^{-1}, because information on this range is not satisfactory. The lack of data is caused by poorly established load acquisition system at this strain rate range. Some load transducers without fluctuations on load–time curves have been proposed. For example, Chuman et al. [22] tried to measure the load of the wide strain-rate range with a sensing block. Unfortunately, the medium strain rate range was not treated in this paper. The present authors are keenly interested in improving the safety of automotive body structure. The maximum strain rate during the frontal crash test is of the order of 10^{3} s^{-1}. Thus, the dynamic strain rate was limited to only 1×10^{3} s^{-1}. For the more precise structural design of the body, the behavior of the medium-strain-rate range is of course very important.

The high-velocity tensile testing machine of a slingshot type adopted the one bar method [23] as a dynamic testing technique. The principle of the one bar method is shown in Fig. 1. It consists of three elements, an impact block as a rigid body, a specimen and an output bar as an elastic bar. Deriving from one-dimensional elastic wave propagation theory and Hooke's law, the fundamental formulae for dynamic stress $\sigma_n(t)$, strain $\varepsilon_n(t)$ and strain rate $\dot{\varepsilon}_n(t)$ in nominal are as follows:

$$\sigma_n(t) = \frac{S_0}{S} E_0 \varepsilon_g\left(t + \frac{a}{c}\right), \tag{1}$$

$$\varepsilon_n(t) = \frac{1}{l}\int_0^t \left\{V(\tau) - c\varepsilon_g\left(\tau + \frac{a}{c}\right)\right\} d\tau, \tag{2}$$

$$\dot{\varepsilon}_n(t) = \frac{1}{l}\left\{V(t) - c\varepsilon_g\left(t + \frac{a}{c}\right)\right\}, \tag{3}$$

where t is the time after impact. l and S are the initial length and cross-sectional area of the specimen, and S_0, E_0 and c are the cross-sectional area, Young's modulus and longitudinal elastic wave velocity of the output bar. $V(t)$ and $\varepsilon_g(t)$ are the velocity of the impact block and the strain of the output bar at the distance a from the loaded end of the bar. In case of dynamic axial compressive tests, Dharan and Hauser [24] derived the same formulae in 1970. Since their projectile was almost rigid and a very small specimen used, the second term in the above Eqs. (2) and (3) was not necessary for their experiments.

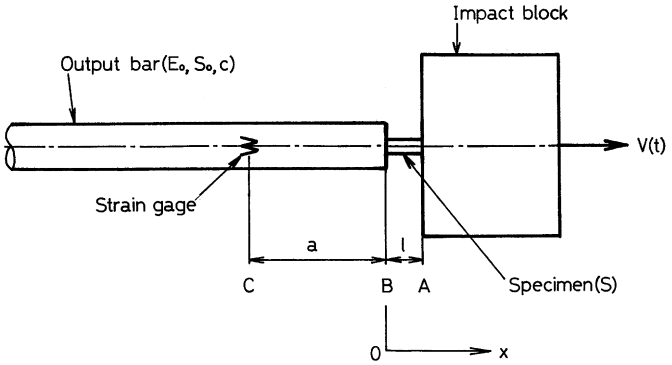

Fig. 1. Principle of the one bar method.

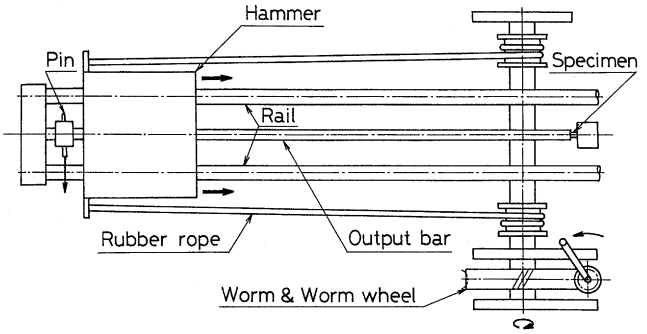

Fig. 2. Schematic drawing of high velocity loading machine of a slingshot type (top view).

The above nominal stress and strain were converted to true representation by the following formulae:

$$\sigma(t) = (1 + \varepsilon_n(t))\sigma_n(t), \tag{4}$$

$$\varepsilon(t) = \ln(1 + \varepsilon_n(t)). \tag{5}$$

The true strain rate was obtained by the following difference equation:

$$\dot{\varepsilon}(t) = \frac{\varepsilon(t + \Delta t) - \varepsilon(t)}{\Delta t}, \tag{6}$$

where Δt is the time interval of the measurement, 1 μs in the present experiments.

Fig. 2 is a schematic drawing (top view) of the high-velocity loading machine of a slingshot type. Powerful rubber ropes connected to a hammer were wound up with a worm gear by hand. The winding generated the elastic force beyond 10 kN in the rubber ropes so that the hammer made of carbon steel, 50 kg in mass, could be accelerated to the velocity of 6–7 m/s. After the winding, the pinned hammer was released by pulling out a pin with a lever. The accelerated hammer impinged on the impact block was made of chromium molybdenum steel. Such a slingshot-driven dynamic

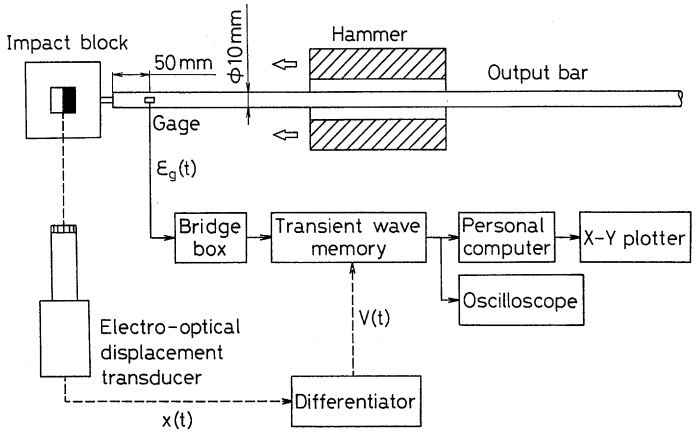

Fig. 3. Block diagram of dynamic data acquisition system for tensile stress–strain relation.

loading system was reported, probably for the first time, by Clark and Duwez [3]. The impact block of 0.66 kg in mass and 60 (W) × 70 (L) × 20 (H) mm in size, flew at the higher velocity, typically 9–11 m/s, than that of the hammer. Therefore, the maximum nominal strain rate attained $1 \times 10^3\ s^{-1}$ with the specimen of the initial gage length of 8 mm.

Fig. 3 shows a block diagram of the dynamic data acquisition system. In order to detect the dynamic strain-time trace $\varepsilon_g(t)$, four semiconductor strain gages (Kyowa KSP-2-120-E3, gage length: 2 mm, gage factor: 120) were cemented onto the output bar made of type 304 stainless steel, at the location of 50 mm apart from the specimen-mounted end. The output bar was 3 m in full length and 10 mm in diameter. The signal was stored in a digital memory (Kawasaki Electronica TMR-100, sampling frequency: 1 MHz, resolution: 10 bits, memory length: 4 kwords). Based on the effective length (2.89 m), density (7910 kg/m^3 [25]) and Young's modulus (196 GPa [25]) of the output bar, 1160 μs was confirmed as the effective duration for measurement. The displacement of the impact block was detected simultaneously with an electro-optical displacement transducer (Zimmer Model 100D/II, gage length of an installed lens: 10 mm). This signal was differentiated with respect to time to obtain the velocity of the impact block $V(t)$, and was stored in another digital memory synchronized with the one for the strain gage signal. Consequently, a stress–strain curve up to fracture was drawn by an $x - y$ plotter via data reduction process in a personal computer. Fig. 4 shows typical traces of $\varepsilon_g(t)$, $V(t)$ and (nominal and true) strain rates calculated by Eqs. (3) and (6). The specimen was one of the investigated steel S15C. The strain rates had a relatively longer rise time, 50–80 μs, and some perturbation was observed. After a peak value, the strain rates decreased by 300–400 s^{-1} at fracture. As a representative of true strain-rate value, the peak values were quoted for the whole curves. However, for upper and lower yield stresses and tensile strength, the strain rates at the instants were adopted, respectively.

Quasi-static tensile tests at three strain rates 1×10^{-3}, 1×10^{-2} and $1 \times 10^{-1}\ s^{-1}$ were conducted with the screw-driven universal material testing machine (Shimadzu AG-10TA, capacity: 98.1 kN). Load was detected by an installed load cell and elongation by two clip gages (Tokyo Sokki Kenkyujo UB-10SL, allowable displacement: 10 mm) with a set of specially designed jigs. Strictly speaking, $1 \times 10^{-1}\ s^{-1}$ is not suitable to refer as quasi-static. The present authors distinguished

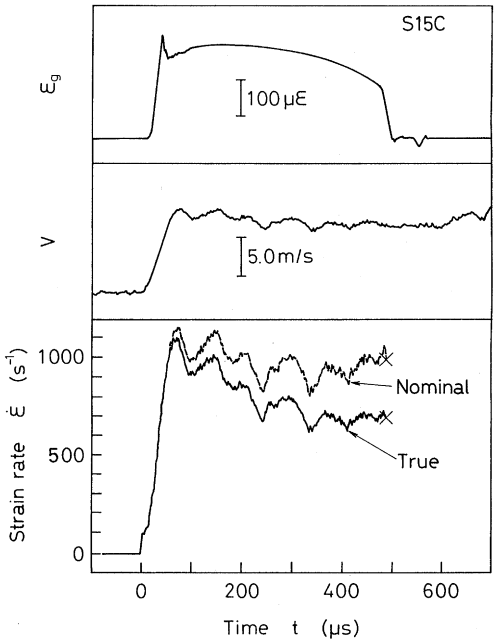

Fig. 4. Typical strain rate-time trace obtained by the one-bar-method apparatus.

these strain rates from the viewpoint of the measuring systems, for convenience, since $\dot{\varepsilon} = 1 \times 10^{-1}\ s^{-1}$ could be dealt with the quasi-static system.

3. Specimen

From JIS G 4051-1979 (Carbon Steels for Machine Structural Use), S15C, S20C, S25C, S35C, S45C and S55C carbon steels were selected for this series of experiments. Symbols for these steels consist of two digits sandwiched between capitals S and C. The two digits indicate a typical C content in a hundred times of the content in wt%. Table 1 tabulates chemical compositions of the steels. The C content of S30C and S35C steels was the same incidentally. However, it was within the allowable range. The steels were supplied as hot drawn cylindrical bars of 13–19 mm in diameter. No heat treatment was done by us. Microstructures of ferrite and pearlite were confirmed by an optical microscope. Average grain diameters were 20–30 μm.

Fig. 5 represents dimensions of the specimen. The initial gage length was 8 mm including round fillets, and diameter 3 mm. Both ends were screw threads for mounting between the impact block and the output bar. These screw threads gave no serious effect on the strain gage signal $\varepsilon_g(t)$. Even after machining, no heat treatment was carried out, in order to maintain commercially available conditions. For the evaluation of the affected zone by the machining, micro-Vickers hardness tests (50 g force was loaded for 30 s) in ferritic grains were executed across the cross-section in the gage length for the softest steel, S15C steel. Fig. 6 indicates that the thickness of the hardened layer by turning was approximately 30 μm. The ratio of the hardened area to the whole cross-section was only 4%. It was negligibly small.

Table 1
Chemical compositions for seven carbon steels

Material	C	Si	Mn	P	S	Cu	Ni	Cr	Al	H	O	N	Fe
S15C	0.14	0.21	0.39	0.008	0.019	0.13	0.05	0.04	0.007	0.0001	0.0022	0.0082	Bal.
S20C	0.19	0.20	0.41	0.012	0.017	0.12	0.08	0.04	0.010	0.0001	0.0020	0.0077	Bal.
S25C	0.22	0.24	0.40	0.006	0.016	0.10	0.06	0.03	0.013	0.0001	0.0015	0.0068	Bal.
S30C	0.33	0.23	0.86	0.023	0.014	0.01	0.02	0.01	0.025	0.0001	0.0024	0.0054	Bal.
S35C	0.33	0.24	0.70	0.008	0.014	0.10	0.04	0.04	0.019	0.0001	0.0019	0.0078	Bal.
S45C	0.44	0.23	0.75	0.010	0.014	0.10	0.04	0.08	0.023	0.0001	0.0017	0.0070	Bal.
S55C	0.54	0.21	0.69	0.011	0.018	0.18	0.05	0.06	0.024	0.0001	0.0017	0.0066	Bal.

(Unit: wt%)

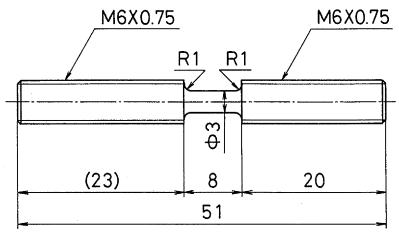

Fig. 5. Specimen dimensions (unit in mm).

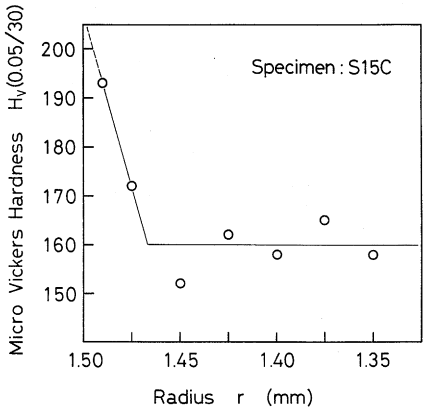

Fig. 6. Micro-Vickers hardness test results across the cross-section in the gage length of S15C steel specimen (The left end of the abscissa is the surface of the specimen.).

4. Results and discussion

Experimental replication was set as three for each experimental condition. The room temperature was 22–25°C at this series of experiments. Fig. 7 depicts typical tensile stress–strain curves for seven carbon steels at two strain rates, (a) $\dot{\varepsilon} = 1 \times 10^{-3}\ s^{-1}$ and (b) $1 \times 10^{3}\ s^{-1}$. Since, under dynamic tension, some of the stress–strain curves were very difficult to recognize their complete ruptures along the curves, the present authors decided to draw them up to zero stress. In case of the quasi-static strain rate (Fig. 7(a)), yield phenomena were getting small, as C content increases. Curves at the other quasi-static rates were essentially similar to this figure. At dynamic strain rate range (Fig. 7(b)), the yield phenomena were enlarged compared to the quasi-static strain rates. Some of the dynamic upper yield points of lower C content steels were higher than the tensile strengths. Klepaczko mentioned that a low alloy steel showed a very high-strain-rate sensitivity of the upper yield stress in excess of the shearing strain rate of $10^{3}\ s^{-1}$. On the other hand, the lower

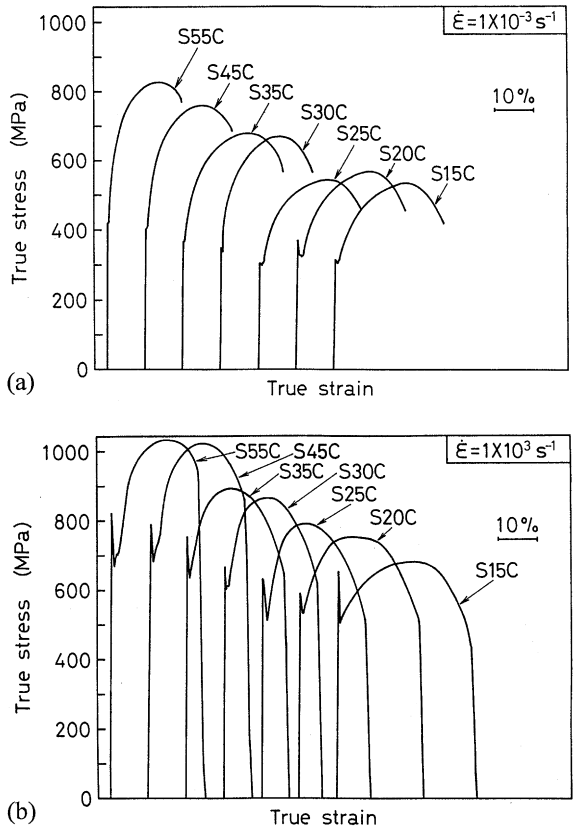

Fig. 7. Typical tensile stress–strain curves for seven carbon steels: (a) $\dot{\varepsilon} = 1 \times 10^{-3}\ s^{-1}$; (b) $\dot{\varepsilon} = 1 \times 10^{3}\ s^{-1}$.

yield stress shows a much lower rate sensitivity with its modified double shear specimen [26]. This fact was able to apply to the present results at several hundreds per strain.

Mechanical characteristic values, i.e., upper yield stress, lower yield stress, tensile strength, uniform strain, local strain, total (breaking) strain and absorbed energy per unit volume were picked up from the stress–strain curves, respectively. Among the characteristic values, the coefficients of variation for tensile strength, total strain and absorbed energy per unit volume were less than 10%. In the above representative values for elongation, the uniform strain (It defined as the strain value at the tensile strength.) is not physically definable. Because, for the initial gage length of the specimen was only 8 mm and the diameter 3 mm, the aspect ratio is only 2.67. Comparing with the axial length of a necked region of the ruptured specimen, the initial gage length was too short so that it was almost impossible to find the part of a non-necked region within the ruptured gage length. Of course, for dynamic tensile/compressive test, such a short specimen is desirable to establish an axially uniform condition in the early stage of the dynamic deformation. Thus, the uniform strain in this work was an apparent quantity.

Fig. 8 shows strain rate and C content dependence of lower yield stress σ_{LY}. By many investigators, at $\dot{\varepsilon} = 10^{-3}$–$10^{-1}\ s^{-1}$, linear relationships between stress and log $\dot{\varepsilon}$ for steels were

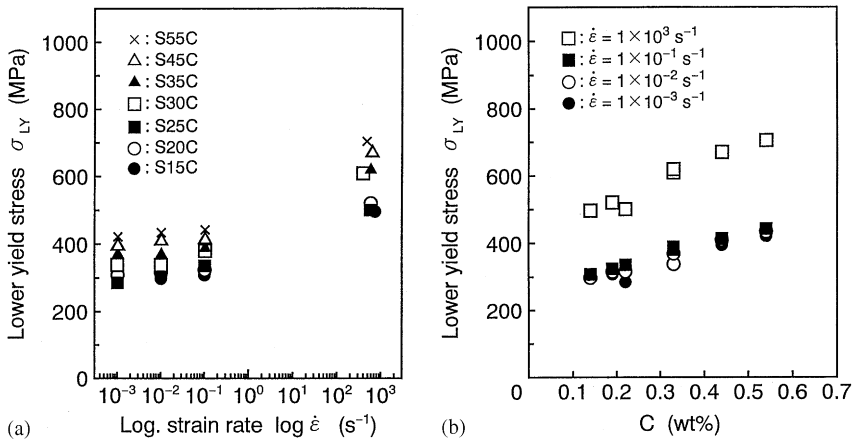

Fig. 8. Strain rate and C content dependence of lower yield stress for seven carbon steels: (a) strain rate dependence; (b) C content dependence.

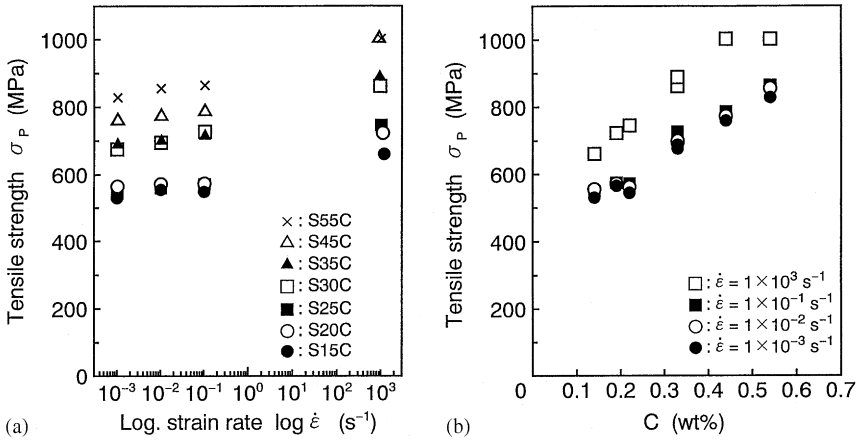

Fig. 9. Strain rate and C content dependence of tensile strength for seven carbon steels: (a) strain rate dependence; (b) C content dependence.

reported. The relationship also held on the present quasi-static range. In case of the dynamic results, however, it hardly held. The expected ratio of the dynamic lower yield stress to quasi-static one was 1.1–1.5, based upon the linear relationship. In fact, the ratio was 1.7–1.8. Harding et al. [8] reported their result indicating the ratio larger than 3. In Fig. 8(b), C content dependence of σ_{LY} was almost linear, even at the dynamic strain rate. This was a rational fact in metallurgy.

Strain rate and C content dependence of tensile strength σ_P is shown in Fig. 9. The same tendencies of σ_{LY} were observed for σ_P. The dynamic stress–strain curves, especially the stress level were affected by adiabatic heating. The temperature rise leads to some softening. This argument will be discussed later. Because for the calculation of the degree of such heating, absorbed energy should be evaluated in advance.

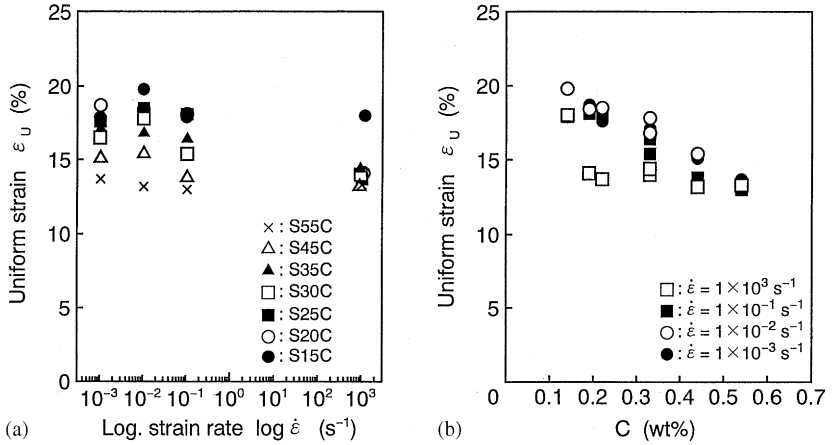

Fig. 10. Strain rate and C content dependence of uniform strain for seven carbon steels: (a) strain rate dependence; (b) C content dependence.

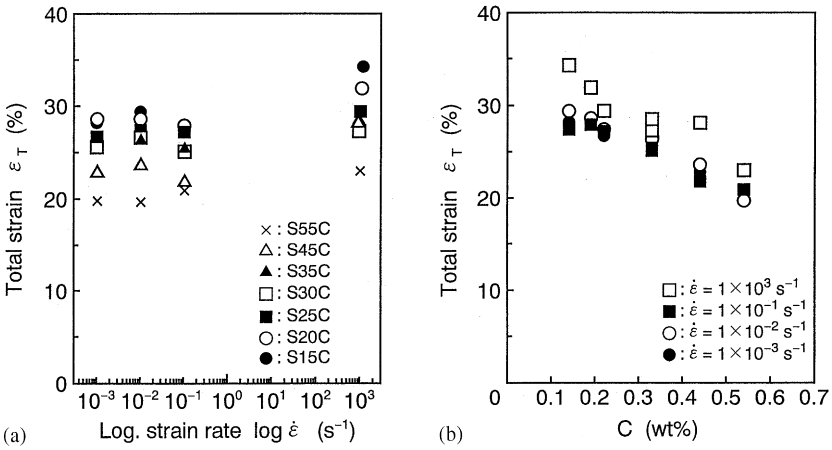

Fig. 11. Strain rate and C content dependence of total (breaking) strain for seven carbon steels: (a) strain rate dependence; (b) C content dependence.

Figs. 10 and 11 represent strain rate and C content dependence of uniform strain (the strain at the tensile strength) ε_U and total (breaking) strain ε_T. Considering their wide scattering, both strains were almost constant over $\dot{\varepsilon} = 1\times10^{-3}$–$1\times10^{-1}$ s^{-1}. In general, at $\dot{\varepsilon} = 1\times10^{3}$ s^{-1}, ε_U decreased while ε_T increased. These contrary tendencies meant that after the occurrence of necking the elongation was not concentrated to the necked part only under dynamic tension. Though the gage length of the specimen was adequately small, plastic wave propagation, reflection and superposition during necking growth might have feasibility to give the contrary tendencies. Both strains were reduced with increasing C content. The gradient of ε_T was almost the same as that of ε_U, except for the dynamic strain rates.

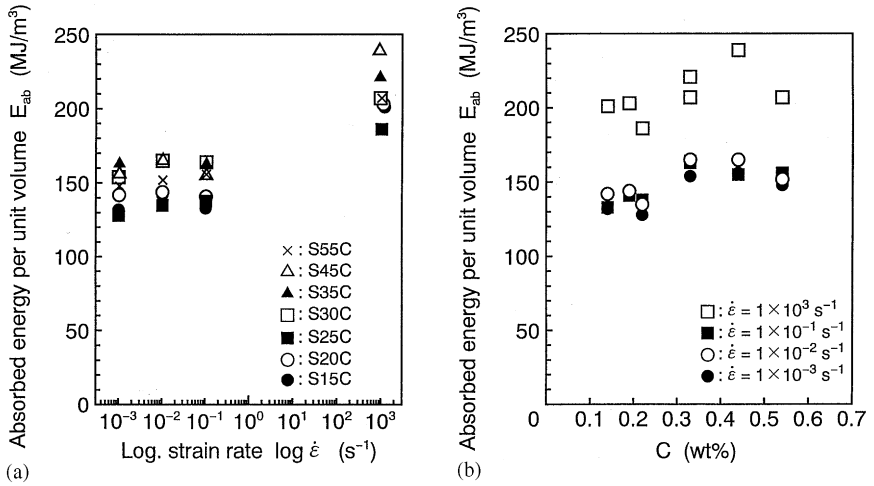

Fig. 12. Strain rate and C content dependence of absorbed energy per unit volume for seven carbon steels: (a) strain rate dependence; (b) C content dependence.

Absorbed energy per unit volume E_{ab} was a measure of toughness. Dependence of strain rate and C content on it is given in Fig. 12. Comparing with quasi-static values, E_{ab} was more than 1.25 times higher under dynamic tension. The C content effect on E_{ab} gave a convex curve at each strain rate. Peak values were obtained at 0.44 wt%C under dynamic tension, and at 0.33 wt%C under quasi-static. In Ref. [21], the present authors formerly reported another series of carbon steels of lower C content (0.033–0.21 wt%C). E_{ab} increased monotonically so that there existed consistency with these results.

The absorbed energy is a factor to evaluate how much the specimen is heated just after dynamic deformation. In the calculation of the temperature rise, the argument of the proportion of work converted to heat β is continuing. In order to solve this problem, temperature measurement technique of very high-frequency response is essential. Macdougall and Harding [27] made a forward movement to obtain the point temperature measurement during dynamic tensile and torsional tests with radiometers of very short-time resolution ~ 1 μs. Their specimen was Ti-6Al-4V alloy of low heat transfer coefficient, 8 W/(m K) [25]. They found that the fracture surface temperature was approximately 200°C just after the dynamic rupture. In case of the present experiments, the temperature rise was not that high. For S45C steel that had the maximum absorbed energy per unit volume at the dynamic strain rate, the temperature rise at rupture can be evaluated by the following equation:

$$\Delta T = \frac{\beta}{c_P \rho} \int_0^{\varepsilon_T} \sigma \, d\varepsilon, \tag{7}$$

where β is the proportion of work converted to heat (1.0, tentatively), c_P is the specific heat at constant pressure (0.492 kJ/(kg K) for medium carbon steel [25]) and ρ is the specific heat (7840 kg/m^3 for medium carbon steel [25]). The integration of the right-hand side equals E_{ab} (239 MJ/m^3). ΔT is evaluated as 62°C. The heat transfer coefficient is 44 W/(m K) [25] for the

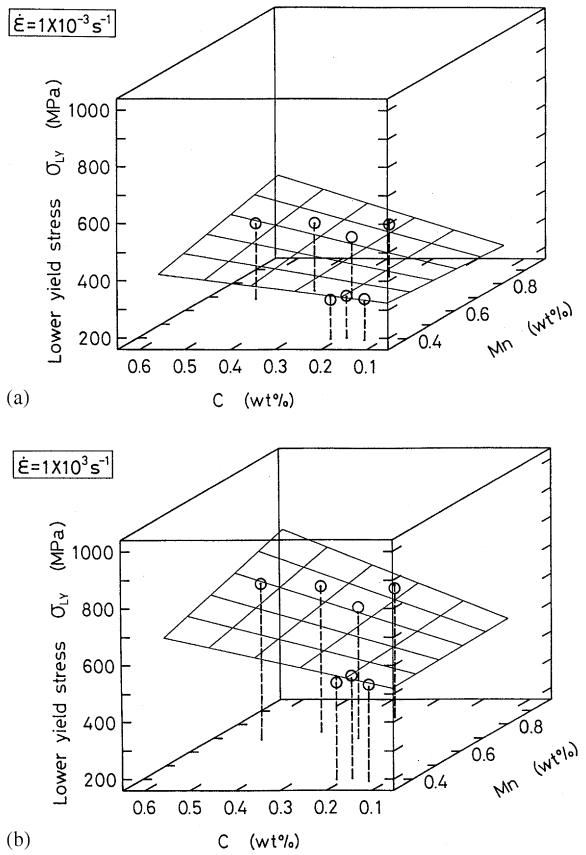

Fig. 13. Predicted surface of lower yield stress for carbon steels by the empirical equation at the strain rates of $1\times10^{-3}\,s^{-1}$ and $1\times10^{3}\,s^{-1}$ (circles are experimental data and dots are predicted values): (a) $\dot{\varepsilon}=1\times10^{-3}\,s^{-1}$; (b) $\dot{\varepsilon}=1\times10^{3}\,s^{-1}$.

steel. This value is much greater than that of Ti-6Al-4V alloy. The temperature gradient in the gage length of the steel specimen was gentler than that of the Ti alloy specimen. Therefore, the softening for dynamically ruptured S45C steel was not so large.

For the strain rate dependence of lower yield stress σ_{LY}, once more attention should be given to the separation of plots at $\dot{\varepsilon}=1\times10^{3}\,s^{-1}$. In Fig. 8(a), two groups of the plots, i.e., a group of S15C, S20C and S25C (0.14–0.22 wt%C), and another group of S30C, S35C, S45C and S55C (0.33–0.54 wt%C) are shown. As indicated in Table 1, the former group contained 0.39–0.41 wt%Mn, the latter 0.69–0.86 wt%Mn. Therefore, it was natural to consider that Mn content also affects the strength level of the carbon steels. In order to combine the effects of C content with that of Mn on σ_{LY}, the following empirical equation [28] was tried to fit:

$$\sigma = k_1 C + k_2 CMn + k_3 Mn + k_4, \tag{8}$$

where C and Mn are the contents of C and Mn, respectively in wt%, and k_i ($i=1, 2, 3$ and 4) are constants. With the least-squares fitting of three linear independent variables, σ_{LY} at

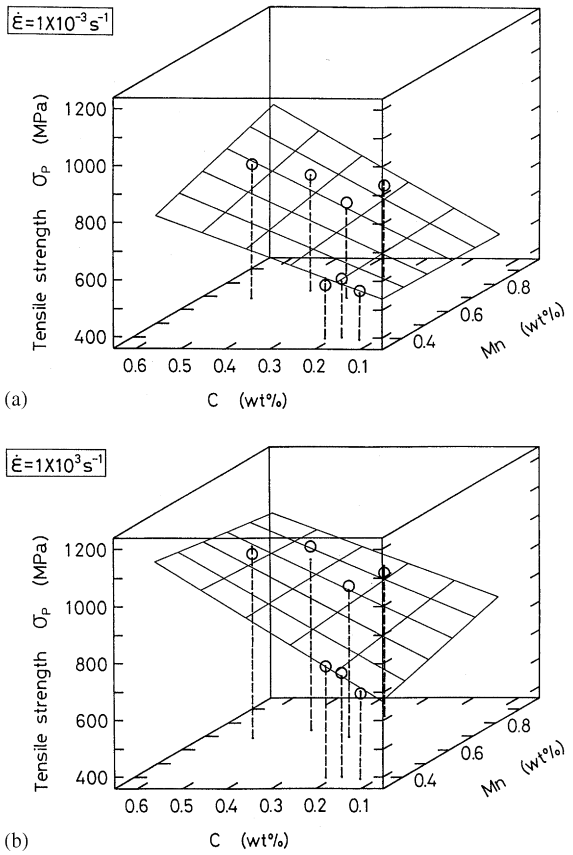

Fig. 14. Predicted surface of tensile strength for carbon steels by the empirical equation at the strain rates of 1×10^{-3} s^{-1} and 1×10^{3} s^{-1} (circles are experimental data and dots are predicted values): (a) $\dot{\varepsilon} = 1 \times 10^{-3}$ s^{-1}; (b) $\dot{\varepsilon} = 1 \times 10^{3}$ s^{-1}.

Table 2
Constants in the empirical equation for predicting strengths of carbon steels

	Strain rate $\dot{\varepsilon}$ (s^{-1})	Constants			
		k_1 (MPa/wt%)	k_2 (MPa/wt%^{2})	k_3 (MPa/wt%)	k_4 (MPa)
Lower yield stress	1×10^{-3}	− 41.5	589	− 139	322
	1×10^{-2}	375	34.7	− 50.2	261
	1×10^{-1}	560	− 398	134	197
σ_{LY} (MPa)	1×10^{3}	149	523	− 39.7	459
Tensile strength	1×10^{-3}	303	661	− 95.1	483
	1×10^{-2}	32.6	1128	− 225	566
	1×10^{-1}	300	651	− 35.9	478
σ_P (MPa)	1×10^{3}	1283	− 779	330	401

$\dot{\varepsilon} = 1 \times 10^{-3}\,\mathrm{s}^{-1}$ and $1 \times 10^{3}\,\mathrm{s}^{-1}$ were predicted in Fig. 13. Hollow circles are the experimental data and the upper dots the predicted ones. Errors were within $\pm 8\%$. The σ_{LY}–C–Mn surfaces indicated a delicate effect of Mn content on the carbon steels. Mn content at higher C content affects σ_{LY} stronger than that at lower C content. Also, tensile strength σ_P was tried to be predicted by Eq. (8). In Fig. 14, good agreement with the experimental results within $\pm 5\%$ was obtained. The constants k_i are tabulated in Table 2 for each case. Such a delicate effect of Mn content on the strengths of the carbon steels at the dynamic strain rate should be considered in better alloy design for developing more crashworthy steels.

5. Conclusions

With the high-velocity tensile loading machine, driven by the elastic energy of the wound-up rubber ropes, and the universal material testing machine, seven carbon steels were tested at four strain rates, 1×10^{-3}, 1×10^{-2}, 1×10^{-1} and $1 \times 10^{3}\,\mathrm{s}^{-1}$. The strain rate and C content dependence of mechanical characteristic values were obtained systematically and analyzed as follows. The linear relationship between stress and logarithmic strain rate did not hold at $1 \times 10^{3}\,\mathrm{s}^{-1}$. The C content effect on the dynamic strength was not that strong as compared with the quasi-static strength. The obtained stress values suggested that Mn was also one of the strongly influential compositions and its effect was amplified with increasing strain rate. In case of elongation for each steel, the dynamic total (breaking) strain was greater than the quasi-static one and uniform strain was vice versa in general. For absorbed energy, maximum values were observed at around 0.44 wt%C under dynamic tension and 0.33 wt%C under quasi-static. From the value of the maximum absorbed energy per unit volume under dynamic tension, the adiabatic heating at approximately 60°C was evaluated. As a case study, from this series of the experiments, an engineering knowledge for the crashworthy alloy design was proposed.

References

[1] Manjoine M, Nadai A. High-speed tension tests at elevated temperatures. Proc ASTM 1940;40:822–37.
[2] Duwez PE, Clark DS. Discussion of the forces acting in tension impact tests of materials. Trans ASME J Appl Mech 1948;15(9):243–7.
[3] Clark DS, Duwez PE. The influence of strain rate on some tensile properties of steel. Proc ASTM 1950;50:560–75.
[4] Taylor GI. The use of flat-ended projectiles for determining dynamic yield stress I. Theoretical considerations. Proc Roy Soc London Ser A 1948;194:289–99.
[5] Whiffin AC. The use of flat-ended projectiles for determining dynamic yield stress II. Tests on various metallic materials. Proc Roy Soc London Ser A 1948;194:300–22.
[6] Jones SE, Drinkard JA, Rule WK, Wilson LL. An elementary theory for the Taylor impact test. Int J Impact Engng 1998;21(1–2):1–13.
[7] Kolsky H. An investigation of the mechanical properties of materials at very high rates of loading. Proc Phys Soc Ser B 1949;62:676–700.
[8] Harding J, Wood EO, Campbell JD. Tensile testing of materials at impact rates of strain. J Mech Engng Sci 1960;2(2):88–96.
[9] Lindholm US, Yeakly LM. High strain-rate testing: tension and compression. Exp Mech 1968;8(1):1–9.
[10] Nicholas T. Tension testing of materials at high rates of strain. Exp Mech 1981;21(5):177–85.

[11] Holzer AJ. A tabular summary of some experiments in dynamic plasticity. Trans ASME J Engng Mater Technol 1979;101(7):231–7.
[12] Malvern LE. The propagation of longitudinal waves of plastic deformation in a bar of material exhibiting a strain-rate effect. Trans ASME J Appl Mech 1951;18(6):203–8.
[13] Seeger A. The mechanism of glide and work hardening in face-centered cubic and hexagonal close-packed metals. In: Fisher JC, Johnson WG, Thomson R, Vreeland Jr T, editors. Dislocations and mechanical properties of crystals. New York: Wiley, 1957. p. 243–329.
[14] Tanaka T, Nojima T. Dynamic and static strength of steels. In: Harding J, editor. Mechanical properties at high rates of strain 1979, Institute of Physics Conference Series No. 47. Bristol and London: Institute of Physics, 1979. p. 166–73.
[15] Johnston WG, Gilman JJ. Dislocation velocities, dislocation densities, and plastic flow in lithium fluoride crystals. J Appl Phys 1959;30(2):129–44.
[16] Gillis PP, Gilman JJ. Dynamical dislocation theory of crystal plasticity I. The yield stress. J Appl Phys 1965;36(11):3370–80.
[17] Gillis PP, Gilman JJ. Dynamical dislocation theory of crystal plasticity II. Easy glide and strain hardening. J Appl Phys 1965;36(11):3380–6.
[18] Hahn GT. A model for yielding with special reference to the yield-point phenomena of iron and related bcc metals. Acta Metal 1962;10(8):727–38.
[19] Kuriyama S, Kawata K. Propagation of stress wave with plastic deformation in metal obeying the constitutive equation of the Johnston–Gilman type. J Appl Phys 1973;44(8):3445–54.
[20] Cowper GR, Symonds PS. Strain hardening and strain-rate effects in the impact loading of cantilever beams. Brown University Division of Applied Mathematics Report No. 28, September 1957.
[21] Kawata K, Miyamoto I, Itabashi M, Sekino S. On the effects of alloy components in the high velocity tensile properties. In: Chiem CY, Kunze H-D, Meyer LW, editors. Impact loading and dynamic behaviour of materials, vol.1. Oberursel: DGM Informationsgesellschaft Verlag, 1988, p. 349–56.
[22] Chuman Y, Mimura K, Kaizu K, Tanimura S. A sensing block method for measuring impact force generated at a contact part. Int J Impact Engng 1997;19(2):165–74.
[23] Kawata K, Hashimoto S, Kurokawa K, Kanayama N. A new testing method for the characterization of materials in high velocity tension. In: Harding J, editor. Mechanical properties at high rates of strain 1979, Institute of Physics Conference Series No. 47. Bristol and London: Institute of Physics, 1979. p. 71–80.
[24] Dharan CKH, Hauser FE. Determination of stress–strain characteristics at very high strain rates. Exp Mech 1970;10(9):370–6.
[25] JSME Mechanical Engineer's Handbook, B4 Engineering Materials. Tokyo: JSME, 1984. p. B4–7 (in Japanese).
[26] Klepaczko JR. An experimental technique for shear testing at high and very high strain rates. The case of a mild steel. Int J Impact Engng 1994;15(1):25–39.
[27] Macdougall DAS, Harding J. The measurement of specimen surface temperature in high-speed tension and torsion tests. Int J Impact Engng 1998;21(6):473–88.
[28] Yajima E, Ichikawa R, Furusawa K. Wakai-gijyutsusha-no-tameno-kikai · kinzoku-zairyo (Structural materials for machines and metallic materials for young engineers). Tokyo: Maruzen, 1979. p. 127 (in Japanese).